Potential-Based Large-Signal Stability Analysis in DC Power Grids With Multiple Constant Power Loads

FANGYUAN CHANG[1] **(Graduate Student Member, IEEE),**
XIAOFAN CUI[2] **(Graduate Student Member, IEEE),**
MENGQI WANG[1] **(Senior Member, IEEE), AND WENCONG SU**[1] **(Senior Member, IEEE)**

[1]Department of Electrical Engineering and Computer Science, University of Michigan-Dearborn, Dearborn, MI 48128 USA
[2]Department of Electrical Engineering and Computer Science, University of Michigan-Ann Arbor, Ann Arbor, MI 48105 USA

CORRESPONDING AUTHORS: M. WANG (mengqiw@umich.edu) and W. SU (wencong@umich.edu)

ABSTRACT The increasing adoption of power electronic devices may lead to large disturbance in DC power grids. Traditionally, the Brayton-Moser mixed potential theory is utilized to address large-signal stability (LSS) analysis. However, this theory proposes sufficient criteria only for large-signal global stability, which provides general but fuzzy information about the stability of DC microgrids. To solve this issue, we propose for the first time a comprehensive hyperlocal large-signal stability analysis (HL-LSS) that is adaptable to large-scale complex power grids. The novel proposed analysis studies the complex situation in nonlinear DC grids with multiple equilibrium points, including stability analysis of each equilibrium point and convergence analysis of state trajectories. The region of attraction (ROA) of microgrids is also estimated.

INDEX TERMS Power electronics-enabled power systems, large-signal stability (LSS), potential theory, constant power loads, multiple-equilibria systems.

NOMENCLATURE

VARIABLES IN MICROGRID MODEL

V_{si}	Input voltage of power converter.
I_{si}	Input current of power converter.
V_{Ci}	Output voltage of power converter.
L_{ti}	Inductance of transmission line in power source side.
I_{ti}	Current through transmission line in power source side.
R_{ti}	Resistance of transmission line in power source side.
I_D	Cumulative current of transmission line in power source side.
C_D	Capacitor at the central point.
V_D	Voltage at the central point.
L_{fj}	Inductance of transmission line in load side.
I_{fj}	Current through transmission line in load side.
R_{fj}	Resistance of transmission line in load side.
V_{Lj}	Output voltage of CPL.
C_{fj}	Capacitor around CPL.
I_{Lj}	Current through CPL.
P_{Lj}	Output power of CPL.
N	The number of branches in power source side.
M	The number of branches in load side.
V_{max}	Maximum output voltage of CPL.
V_{min}	Minimum output voltage of CPL.

I_{max}	Maximum output current of CPL.
I_{min}	Minimum output current of CPL.
V_{refi}	Equivalent voltage source of power converter.
R_{pi}	Parallel resistance of converter controller.
R_{qi}/L_{qi}	Impedance of converter controller.
I_{pi}	Current through the parallel resistor of converter controller.
I_{qi}	Current through the impedance of converter controller.

VARIABLES IN POTENTIAL ANALYSIS

$A/B/C/k$	Coefficients of state equation.
x	State vector.
y	Output vector.
u	Input vector.
I	Identity matrix.
$P(x)$	Potential function.
J	Component matrix.

I. INTRODUCTION

WITH high penetration of power electronic devices, DC power grids are moving towards smarter and more

competitive grids in recent years. A significant number of today's electrical loads are running on DC power, so supplying them from a DC source would simplify the power circuit and save energy overall [1]. Especially, DC microgrids widely attract people's interest due to their advantages in operation and control. However, the characteristics of Power-Voltage coupling and low inertia of DC microgrids increase the risks of grid instability. In conventional bulk power systems, the rotor inertia and the damping properties of synchronous generators play a significant role in stabilizing the system. Compared with the conventional power plants dominated by synchronous generators, the converter-interfaced distributed generator (DG) and renewable energy source (RES) have either a very small or no rotating mass, which is the main source of inertia [2]. With the growing penetration of DGs/RESs, the low inertia and damping effect is increasingly destabilizing the power grid. Moreover, in DC power grids, the stored energy in bus capacitors is much less than the rotating storage of the rotation axis [3]. Therefore, the stability of DC power grids deteriorates easily from the disturbance due to low inertia and poor damping [4]–[6]. Power grids with a large percentage of constant power loads (CPLs) on the load side are especially potentially destabilized by these elements, no matter whether in DC microgrids or in hybrid AC/DC systems [7]. The reason is that a CPL always exhibits negative incremental impedance in circuits [8]. Therefore, it is necessary to promote stability analysis and novel control strategies for enhancing microgrid stability.

There is a large amount of literature about stability analysis in DC power grids, which can be categorized as follows according to the type of disturbance taken into consideration. Many existing studies were performed using *small-signal models* based on linearization; however, the methodology has limited applicable scenarios. For example, the studies in [9]–[11] impose classical eigenvalues analysis on linearized models, which may not always be feasible considering the common large disturbances that occur in power grids, such as pulse faults and load switching. Small-signal stability (SSS) can determine the system stability only at a nearby equilibrium point. Relatively, large-signal stability (LSS) analysis can determine the stable condition for power systems with large disturbances, such as load switching, pulse power loads, and faults. In paper [12], several tools of LSS analysis of DC power systems are reviewed, including the second method of Lyapunov applied to multi-models, Brayton–Moser's nonlinear potential method, block diagonalized quadratic Lyapunov function (BDQLF), reverse trajectory tracking, etc. The LSS analysis optimizes the design of power grid in terms of system stability. In [13], the authors develop an LSS analysis of a circuit system with a single converter with Takagi-Sugeno multi-modeling [14]. Paper [15] presents the destabilizing effect of CPLs in microgrids and compare a significant difference between SSS and LSS analyses. The limitation of this research is that the proposed model includes only one power source and CPL.

Recently, many studies on grid stability have been performed from the perspective of large-signal stability analysis using the Brayton-Moser potential theory [16]. For example, the study in [18] designs criteria for distributed load systems with one single power source and CPLs to guarantee stability during large disturbances. The criteria are based on Lyapunov stability, Brayton-Moser potential theory, and the existence of equilibrium points. In paper [19], the authors discuss the dynamic behavior of a hybrid AC/DC electric system under large disturbances, which is a typical power distribution network being developed for future aircraft. The studied power system includes a single equivalent CPL with structure simplification. Brayton-Moser potential theory is leveraged along with Lyapunov stability theorems to determine an analytical estimation of large-signal stability boundary. Unfortunately, many studies under this topic are flawed due to a deficient understanding of the Brayton-Moser potential theory. For example, the definition of potential in [20], [21] is questionable because it violates a theoretical foundation of the potential theory, namely, that the potential theory is well-constructed only in *autonomous systems* and is independent of the state trajectories. In addition, the limitations of the original Brayton-Moser potential theory are mitigated in our study [22].

In general, the original potential theory has a creative and strategic construction, and it is very useful in LSS analysis in multiple types of nonlinear circuits. However, its limitations also should be noted. The original potential theory proposes sufficient criteria only for large-signal global stability, which provides general but unclear information about grid stability. It works well for DC microgrids with a single CPL and a single equilibrium point, but for DC microgrids with multiple CPLs and equilibrium points, it cannot determine the stability of each equilibrium point or differentiate trajectories with different starting states. In a complex microgrid system, it is always necessary to obtain precise information about every equilibrium point and trajectory. With such information, a region of attraction (ROA) of the system can be estimated, which can ensure safe system operation in the event of a large disturbance.

Therefore, we propose in this paper hyperlocal large-signal stability analysis (HL-LSS) targeted at DC microgrids with multiple CPLs and equilibrium points. The definition of the conventional LSS is that there exists at least one stable equilibrium point of the dynamic system at which any subsequent trajectories of a set of initial conditions end up. However, it cannot provide accurate stability information in microgrids with multiple equilibrium points because state trajectories from different initial states may converge to different equilibrium points. In fact, the difference in the stability of each equilibrium point leads to a more complicated situation. In a microgrid with multiple equilibrium points, an equilibrium point is defined as HL-LSS if there exists a *subset* of the domain in which any subsequent trajectories starting from this subset converge to the equilibrium point. This definition emphasizes the stability of each equilibrium point and

differentiates the convergences of state trajectories with different starting points, which is more appropriate and practical in microgrids with multiple equilibrium points.

In a nutshell, LSS in DC microgrids is still an unsolved issue. This paper presents a systematic approach to solve this issue. The contributions of this paper are summarized as follows:

1) We model the DC microgrids with high penetration of power electronic devices and multiple CPLs based on potential theory. 2) We propose the definition of HL-LSS in complex DC microgrids with multiple equilibrium points. Based on the definition, we study the stability of each equilibrium point and the convergence of state trajectories with different starting points using the proposed novel potential-based approach. We integrate the discussion of the local stability of each equilibrium point in the large-signal global stability analysis of the system. 3) The ROA of a microgrid system is estimated to investigate the local stability of each equilibrium. The proposed potential-based ROA estimation has a lower computation cost compared with the traditional ROA estimation method. 4) We resolve misunderstandings and emphasize the key points of potential theory, which plays a fundamental role in LSS analysis in nonlinear power grids.

The paper is organized as follows. In section II and section III, the model of DC microgrids and some concepts of stability are described. In section IV, we model the dynamics of DC microgrids and formulate equilibrium analysis using the potential-based approach. Additionally, we correct some misunderstandings of the potential theory in existing literature. In Section V, we estimate the ROA of the proposed DC microgrid model. Section VI verifies our theoretical derivation with a simulation-based study.

II. MODEL ASSUMPTIONS
A generalized circuit structure of a DC microgrid can be described in Fig. 1. Without loss of generality, the circuit diagram is modeled based on the following assumptions:
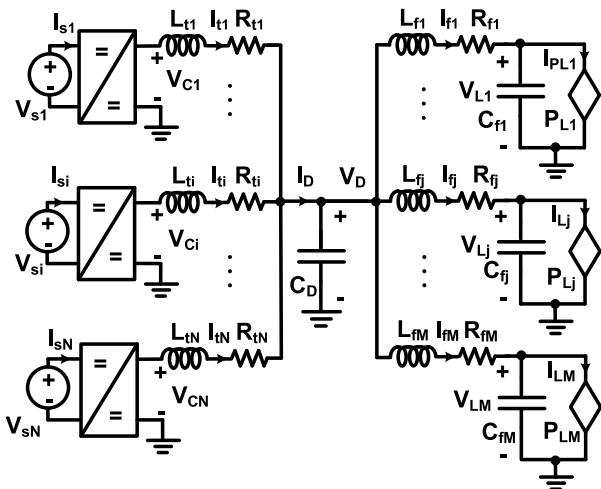

FIGURE 1. The general circuit structure of a typical DC microgrid.

1) The power supplies are all constant voltage sources. 2) The DC-DC converters are utilized to step up/down voltage. They can be ideal buck converters or boost converters. No parasitic element is considered. Moreover, the modeling of power converters is formulated with the state space averaging method. 3) The transmission lines are modeled as pure impedances. L_{ti}, R_{ti} and $L_{fj}, R_{fj}(i = 1, 2, \ldots, N, j = 1, 2, \ldots, M)$ in Fig. 1 represent the impedances of transmission lines in power source side and demand side, respectively. 4) The demand side consists of multiple CPLs. The model of the CPL is shown in Fig. 2(a) and its operation follows the following function:

$$\begin{cases} I_{PL} = I_{max}, & V_L \leq V_{min} \\ V_L = \dfrac{P_L}{I_{PL}}, & V_{min} \leq V_L \leq V_{max} \\ V_L = V_{max}, & I_{PL} < I_{min} \end{cases} \quad (1)$$
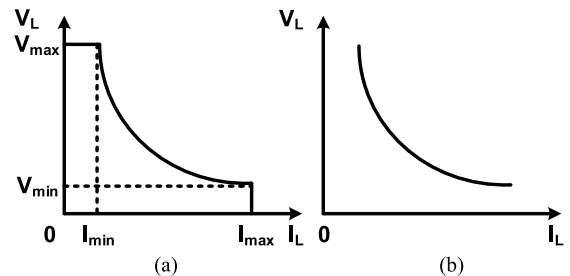

FIGURE 2. The models of a CPL: (a) a realistic one with the operational upper bounds; (b) a traditional one without the operational upper bounds.

The CPL model in Fig. 2(a) has operation bounds on voltage and current, with the consideration of the practical operation of CPLs in DC microgrids. In practice, a parallel diode of CPL clamps the voltage as a non-negative value. Notably, all mathematical prerequisites of the LaSalle theorem can be satisfied by this model, which provides a fundamental principle of the potential theory for LSS of nonlinear circuits. In most of the existing studies about microgrid stability, the conventional CPL model without current or voltage limits is utilized, as shown in Fig. 2(b). However, this model does not fit for potential-based stability analysis since it violates the prerequisites of the LaSalle theorem, which requires the domain of the studied dynamic system to be a compact positively invariant set [23]. The domain of the traditional CPL model shown in Fig 2. (b) is the set of non-zero positive real numbers $\mathcal{R}_+^*$, which is an open set, so the requirements cannot be satisfied.

III. STABILITY DESCRIPTION IN DC MICROGRIDS
A large disturbance could happen in power grids when a fault or load switching occurs. Regrettably, traditional SSS analysis, which deploys the small-signal and linearized model, cannot provide sufficient information about the stability of a microgrid with CPLs involving a large disturbance. Another

limitation of SSS analysis is that power converter dynamics can be approximated by a state-space averaging model only if the system bandwidth is lower than switching frequency [22], [24].

LSS analysis is able to determine safe operation conditions in practical DC microgrids even when they are going through a large disturbance. The definition of the traditional LSS is that there exists at least one stable equilibrium in the dynamic system where any subsequent trajectories of a set of initial conditions end up. For microgrids with a single equilibrium point, we can derive sufficient conditions for their global large-signal stability (G-LSS), which guarantees LSS of the microgrid for any initial states in the *complete domain*. However, G-LSS is not applicable to a microgrid with multiple equilibrium points because state trajectories with different initial states may converge to different equilibrium points. To solve this issue, we propose in this paper a definition of HL-LSS for microgrids with multiple equilibrium points. In a microgrid with multiple equilibrium points, an equilibrium point is called HL-LSS if there exists a *subset* of the domain from which any subsequent trajectories starting from this subset converge to the equilibrium point. This concept places emphasis on the stability of each equilibrium and differentiates the convergences of state trajectories with different starting points, which is more appropriate and practical in microgrids with multiple equilibrium points. The HL-LSS is different from the traditional local stability in SSS analysis for the following two reasons: first, HL-LSS is developed on the original nonlinear system, whereas local stability in SSS analysis depends on a small-signal and linearized system; second, there exists ROA for every equilibrium point with HL-LSS, while local stability in SSS analysis cannot provide ROA. The relationships of the above concepts are depicted in the following figure.
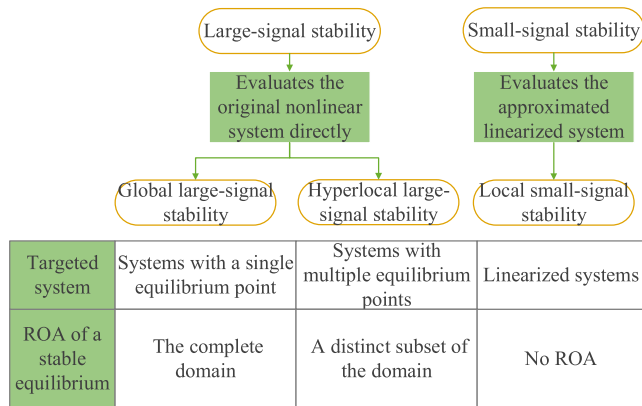

FIGURE 3. The relationships among different types of stability.

In conclusion, the HL-LSS of DC microgrids with multiple CPLs is proposed and discussed. We study the stability of each equilibrium point in microgrids with multiple equilibrium points using a potential-based approach. The ROA for each stable equilibrium point is also estimated.

IV. DC MICROGRIDS MODELING AND EQUILIBRIA ANALYSIS

A. MICROGRIDS MODEL WITH POWER CONVERTER CONTROLLERS

The general framework of a DC microgrid is shown in Fig. 1. In a DC microgrid, reasonable control of power converters can smooth the power flow and provide electric power with high quality through the regulation of output voltage. Considering the distinctive advantages of current-mode control, we build a novel type of converter controller, shown in the following figure. The applied droop-inertia controller is first proposed and explained in our paper [22]. Compared to the traditional droop controller often deployed in DC microgrids, the droop-inertia controller shows more stable characteristics and smaller steady-state errors. Moreover, it can be noted that the droop-inertia controller degrades to a traditional droop controller when $L_{qi} = 0$.

The droop-inertia controller regulates the output voltage V_{Ci} to the given reference value V_{refi} by controlling the inductor current I_{si}. The admittance block transfers the signal of voltage error $V_{refi} - V_{Ci}$ to a current signal I_{ei}. The feature of the current controller is to regulate I_{si} according to the input I_{ei}. It is worth mentioning that the regulation of I_{si} is realized by control of the duty ratio of the transistor. The current controller is designed as a proportional integral (PI) controller here, which regulates the duty ratio based on the current difference $I_{ei} - I_{si}$. Both the droop-inertia controller and the current controller are linear controllers. The transfer function of the droop-inertia controller is as follows:

$$G(s) = \frac{I_{si}(s)}{V_{refi}(s) - V_{Ci}(s)} = Y_{in}(s) = \frac{R_{pi} + sL_{qi} + R_{qi}}{R_{pi}(sL_{qi} + R_{qi})} \quad (2)$$

where Y_{in} is the equivalent admittance of the block in Fig. 5.

Considering the above DC microgrid modeling analysis, it is not necessary to discuss the LSS of the converter side. The reason is explained as follows. The modeling of power converters is formulated with the state space averaging method. Moreover, by designing the bandwidth of the current control loop to be much higher than the voltage control loop, we can view the voltage control loop as a linear system that consists of both the power converter and the droop-inertia controller. Note that these two assumptions are based on the concept of time-scale separation, which is commonly used in the design of power electronics controllers; they are not based on linearization. Based on these assumptions, the power converter plant can be modeled as a linear system. The SSS is the same as the LSS in linear models. Therefore, the discussion of LSS of the converter side is not necessary.

The equivalent circuit of the model in Fig. 4 is shown in Fig. 6. The state equations of the model in Fig. 6 are shown as follows:

$$\begin{cases} \dot{x} = Ax + Bu + k \\ y = Cx \\ y_j u_j = -P_{Lj}, \quad \forall j \in \{1, 2, \dots, M\} \end{cases} \quad (3)$$
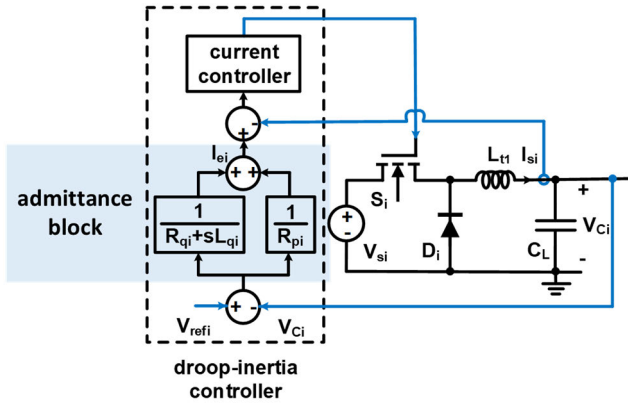
FIGURE 4. The circuit diagram of a power converter with droop-inertia controller.
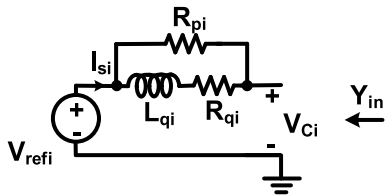

FIGURE 5. The equivalent circuit of the proposed converter controller.
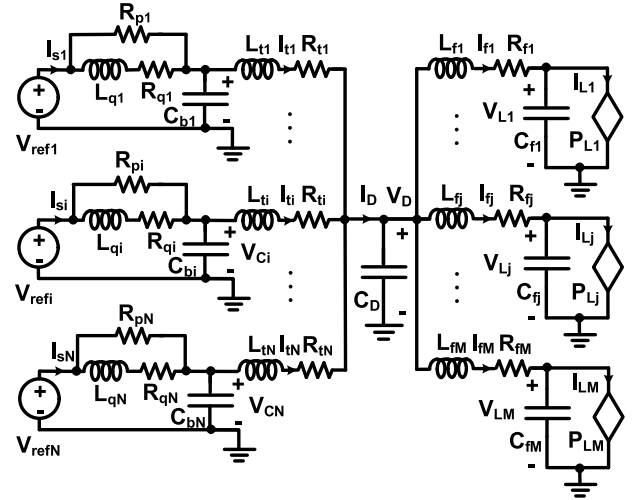

FIGURE 6. The equivalent model of a DC microgrid under current-mode control.

B. STEADY-STATE ANALYSIS OF DC MICROGRIDS WITH MULTIPLE CPLs

Firstly, we solve equilibrium points of the given microgrid system. The state equations of the model in Fig. 6 are described in (3). Let $\dot{x} = 0$. The equilibria of the system $(\bar{x}, \bar{y})$ is solved as

$$\begin{cases} \bar{x} = -A^{-1}(B\bar{u} + k) \\ \bar{y} = -CA^{-1}(B\bar{u} + k) \end{cases} \tag{4}$$

with the assumption that A^{-1} exists.

In fact, this assumption holds in our case. The explanation is as follows. Suppose a matrix T, whose size is the same as A. x, u, k are defined in the above section. The solvability and the existence of the equilibria of the original system are undetermined due to the complexity of nonlinear circuit systems. However, whether A is invertible depends only on the circuit structure without the CPLs and whether x is a minimal realization. Hence, A is invertible because the DC system without the CPLs is a linear time invariant (LTI) system and x is a minimal realization. The superposition theorem [25] in linear circuit systems is adopted here to clarify the explanation. The input u in our model consists of current sources; the constant term k consists of voltage sources; and

where $x = [I_{q1}, \ldots, I_{qN} \; I_{t1}, \ldots, I_{tN} \; I_{f1}, \ldots, I_{fM} \; V_{C1}, \ldots, V_{CN} \; V_D \; V_{L1}, \ldots, V_{LM}]^T$, $u = [-I_{L1}, \ldots, -I_{LM}]^T$, $y = [V_{L1}, \ldots, V_{LM}]^T$,

A and k are shown in one-column form at the bottom of this page because of the large size,

$$B = \begin{bmatrix} 0_{(3N+M+1)\times M} \\ diag\{\frac{1}{C_{f1}}, \ldots, \frac{1}{C_{fM}}\} \end{bmatrix},$$

$C = \begin{bmatrix} 0_{M\times(3N+M+1)} & I_{M\times M} \end{bmatrix}$, (where I is the identity matrix),

$$i \in \{1, 2, \ldots, N\}, j \in \{1, 2, \ldots, M\}.$$

I_{qi} is the current through the resistor R_{qi}, and other notations are as notated in Fig. 6.

$$A = \begin{bmatrix} diag\{-\frac{R_{q1}}{L_{q1}}, \ldots, -\frac{R_{qN}}{L_{qN}}\} & 0_{N\times N} & 0_{N\times M} & diag\{-\frac{1}{L_{q1}}, \ldots, -\frac{1}{L_{qN}}\} & 0_{N\times 1} & 0_{N\times M} \\ 0_{N\times N} & diag\{-\frac{R_{t1}}{L_{t1}}, \ldots, -\frac{R_{tN}}{L_{tN}}\} & 0_{N\times M} & diag\{\frac{1}{L_{t1}}, \ldots, \frac{1}{L_{tN}}\} & [-\frac{1}{L_{t1}}, \ldots, -\frac{1}{L_{tN}}]^T & 0_{N\times M} \\ 0_{M\times N} & 0_{M\times N} & diag\{-\frac{R_{f1}}{L_{f1}}, \ldots, -\frac{R_{fM}}{L_{fM}}\} & 0_{M\times N} & [\frac{1}{L_{f1}}, \ldots, \frac{1}{L_{fM}}]^T & diag\{-\frac{1}{L_{f1}}, \ldots, -\frac{1}{L_{fM}}\} \\ diag\{\frac{1}{C_{b1}}, \ldots, \frac{1}{C_{bN}}\} & diag\{-\frac{1}{C_{b1}}, \ldots, -\frac{1}{C_{bN}}\} & 0_{N\times M} & diag\{-\frac{1}{R_{p1}C_{b1}}, \ldots, -\frac{1}{R_{pN}C_{bN}}\} & 0_{N\times 1} & 0_{N\times M} \\ 0_{1\times N} & [\frac{1}{C_D}, \ldots, \frac{1}{C_D}]_{1\times N} & [-\frac{1}{C_D}, \ldots, -\frac{1}{C_D}]_{1\times M} & 0_{1\times N} & 0 & 0_{1\times M} \\ 0_{M\times N} & 0_{M\times N} & diag\{\frac{1}{C_{f1}}, \ldots, \frac{1}{C_{fM}}\} & 0_{M\times N} & 0_{M\times 1} & 0_{M\times M} \end{bmatrix},$$

$$k = \begin{bmatrix} V_{ref1}/L_{q1}, \ldots, V_{refN}/L_{qN} & 0_{1\times N} & 0_{1\times M} & V_{ref1}/R_{p1}C_{b1}, \ldots, V_{refN}/R_{pN}C_{bN} & 0 & 0_{1\times M} \end{bmatrix}^T$$

$\bar{x}$ consists of different inductor currents, capacitor voltages, and load voltages. At one moment, the CPLs can be treated as current sources. According to the following equation, every element in matrix T can be determined by solving a linear circuit with only one independent power source and then adding them algebraically. T exists and is unique based on the property of circuit systems.

$$\bar{x} = -T(B\bar{u} + k) \tag{5}$$

Considering the state equation at the equilibria $A\bar{x} = -(B\bar{u}+k)$ and the above equation $\bar{x} = -T(B\bar{u}+k)$, we have

$$TA\bar{x} = -T(B\bar{u} + k) = \bar{x} \tag{6}$$

that is, $TA = I$. Therefore, A^{-1} exists.

Next, we continue to solve the equations

$$\begin{cases} \bar{x} = -A^{-1}(B\bar{u} + k) \\ \bar{y} = -CA^{-1}(B\bar{u} + k) \end{cases} \tag{7}$$

Notate $G = -CA^{-1}B = [g_1, \ldots, g_M]^T$; $O = -CA^{-1}k = [o_1, \ldots, o_M]^T$; g_j are the column vectors with size $(3N + 2M + 1) \times 1, \forall j \in \{1, 2, \ldots, M\}$, $\bar{y} = [\bar{y}_1, \ldots, \bar{y}_M]^T, \forall j \in \{1, 2, \ldots, M\}$.

From the above equations, we have

$$\bar{y}_j = g_j^T \bar{u} + o_j, \quad \forall j \in \{1, 2, \ldots, M\} \tag{8}$$

Considering the equation $y_j u_j = -P_{Lj}, \forall j \in \{1, 2, \ldots, M$, we have

$$(g_j^T \bar{u} + o_j)u_j = -P_{Lj}, \quad \forall j \in \{1, 2, \ldots, M\} \tag{9}$$

The group of equations can be written in the following form:

$$\bar{u}^T F_2^{(j)} \bar{u} + F_1^{(j)} \bar{u} + F_0^{(j)} = 0, \quad \forall j \in \{1, 2, \ldots, M\} \tag{10}$$

where $F_2^{(j)}$ is the coefficient matrix with the size $(3N + 2M + 1) \times (3N + 2M + 1)$, whose j-th column is g_j and other columns are all zero vectors; $F_1^{(j)}$ is a vector with size $1 \times (3N + 2M + 1)$, whose j-th element is o_j and other elements are all zero; $F_0^{(j)}$ is a constant in which $F_0^{(j)} = P_{Lj}, \forall j \in \{1, 2, \ldots, M\}$.

Therefore, we conclude that there exist equilibrium point(s) in the microgrid system if equation (10) is solvable. In engineering practice, the solvability of equation (10) can be known by solving it using optimization solvers. In fact, the condition that an optimization solver obtains a solution of equation (10) is a sufficient but not necessary condition for the existence of an equilibrium point. More studies about the solvability and existence of equilibria in similar dynamic systems can be found in [26], [27]. In this paper, we assume that equation (10) is solvable and that there exists at least one equilibrium for further discussion of ROA.

Here, we take the case with two CPLs as an illustrative example. Given $N = 1, M = 2$, we obtain the specified state equations for the example from equation (11):

$$\begin{cases} P_1 = V_{eq} \cdot I_{P1} - I_{P1}^2 (R_{eq} + R_{f1}) - R_{eq}I_{P1}I_{P2} & (a) \\ P_2 = V_{eq} \cdot I_{P2} - I_{p2}^2 (R_{eq} + R_{f2}) - R_{eq}I_{P1}I_{P2} & (b) \end{cases} \tag{11}$$

TABLE 1. Microgrid Model parameters (The unit: V, Ohm, W).

V_{eq}	200	P_1	900	R_{f1}	0.7
R_{eq}	0.3	P_2	500	R_{f2}	0.9

From another perspective, the equations can be verified by the power balancing equations of the Thevenin equivalent circuit of the microgrid model shown in Fig. 6. The microgrid in Fig. 6 has the following Thevenin equivalent model when it is in steady state:

where V_{eq} is the equivalent voltage, R_{eq} is the equivalent resistor.

Notate $x = [I_{P1}, I_{P2}]^T$. The above equations can be transformed to the following quadratic form to determine their shape.

$$x^T A x + bx + c = 0 \tag{12}$$

where $A = \begin{bmatrix} R_{eq} + R_{f1} & R_{eq}/2 \\ R_{eq}/2 & 0 \end{bmatrix}, b = [-V_{eq} \ 0], c = P_1$.

Suppose $Q = [v_1 \ v_2]$, where v_1 and v_2 are eigenvectors of A; $\Lambda = diag([\lambda_1 \ \lambda_2])$, where λ_1 and λ_2 are the corresponding eigenvalues of v_1 and v_2, respectively. Considering that A is a real symmetric matrix, we can decompose A as follows:

$$A = Q \begin{bmatrix} \lambda_1 & 0 \\ 0 & \lambda_2 \end{bmatrix} Q^{-1} = Q \begin{bmatrix} \lambda_1 & 0 \\ 0 & \lambda_2 \end{bmatrix} Q^T \tag{13}$$

Equation (13) can be converted to

$$y^T Q^T A Q y + bQy + c = 0 \tag{14}$$

where $y = Q^{-1}x$. Notate $y = [I'_{P1} \ I'_{P2}]^T$. Then we have

$$\lambda_1 I_{P1}'^2 + \lambda_2 I_{P2}'^2 + [-V_{eq} \ 0][v_1 \ v_2][I'_{P1} \ I'_{P2}]^T = -P_1 \tag{15}$$

Notate $[r_1 \ r_2] = [-V_{eq} \ 0][v_1 \ v_2]$. The above equation can be converted to

$$\lambda_1(I_{P1}' + \frac{r_1}{2\lambda_1})^2 + \lambda_2(I_{P2}' + \frac{r_2}{2\lambda_2})^2 = \frac{r_1^2}{4\lambda_1} + \frac{r_2^2}{4\lambda_2} - P_1 \tag{16}$$

Solving the eigenvalues of A, we obtain that

$$\lambda_{1,2} = \frac{R_{eq} + R_{f1} \pm \sqrt{2R_{eq}^2 + 2R_{eq}R_{f1} + R_{f1}^2}}{2} \tag{17}$$

We know that $\lambda_1 > 0, \lambda_2 < 0$ (suppose $\lambda_1 > \lambda_2$). Therefore, equation (12-a) is a hyperbola. Similarly, it is concluded that equation (12-b) is also a hyperbola.

An example is taken to illustrate the shape of the state equations in (12) and to develop equilibria analysis. Suppose a DC microgrid model with the following Thevenin-equivalent parameters.

The state equations of this model in (12) are plotted in Fig. 8. The difference in the operation boundaries of the CPL model may generate different operation scenarios. Here, four different operation scenarios are discussed.
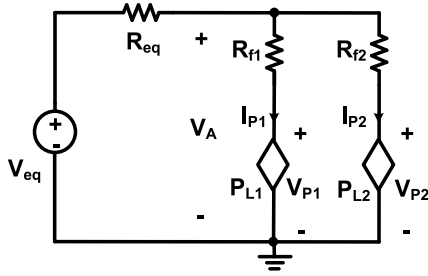
FIGURE 7. Thevenin equivalent model of a DC microgrid with multiple CPLs.
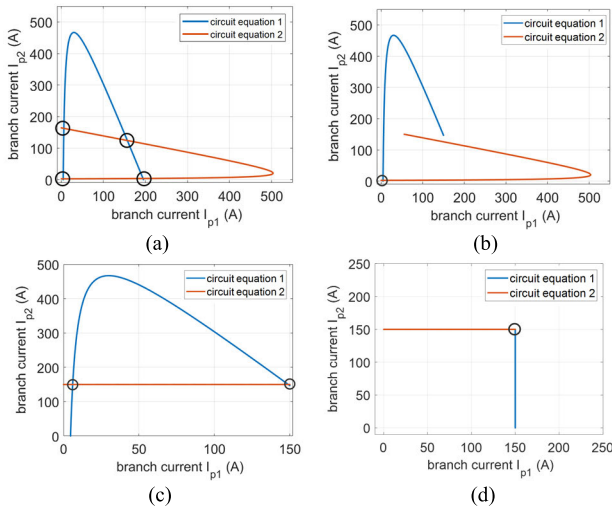

FIGURE 8. Visualization of power balancing equations in (12).

1) A SPECIAL LIMITING CASE WHERE THE PARAMETERS OF THE CPL MODEL SATISFY THAT $\lim V_{min} \rightarrow 0, \lim I_{max} \rightarrow \infty$

This case is shown in Fig. 8(a). It can be observed that there are four equilibrium points in this system.

2) THE PARAMETERS OF THE CPL MODEL I_{max} AND V_{min} ARE FINITE

2-a) Suppose that the maximum operation current of the two CPLs is $I_{max} = 150A$. In Fig. 8(b), both CPLs operate as the function $V_L = P_L/I_{PL}$. There exists only one equilibrium point in this case.

2-b) In Fig. 8(c), only one CPL operates as the function $V_L = P_L/I_{PL}$. Another CPL operates as the function $I_{PL} = I_{max}$, which means it actually works as a current source. There are two equilibrium points in this system.

2-c) In Fig. 8(d), both CPLs operate as the function $I_{PL} = I_{max}$, i.e., both CPLs work as current sources. In this case, there exists only one equilibrium point.

C. POTENTIAL FUNCTION OF DC MICROGRIDS MODEL

First, we show the definition of the potential function.

Definition (Potential Function [28]): Suppose there are r inductors, s capacitors, and b nonlinear resistors and power

supplies in total in a circuit system. These components are sequentially numbered, starting from inductors and capacitors to resistors and power supplies, notated by μ. Then we define the potential function $P(i, v)$ of the above circuit system as

$$P(i, v) = \sum_{\mu=r+1}^{r+s} v_\mu i_\mu |_\Gamma + \sum_{\mu>r+s}^{r+s+b} \int_\Gamma^{v_\mu di_\mu} \quad (18)$$

where v_μ and i_μ are voltage and current of element μ, respectively. Regarding the notations of the elements, $1, 2, \ldots, r$ represent inductors; $r + 1, \ldots, r + s$ represent capacitors; $r + s + 1, \ldots, r + s + b$ represent nonlinear resistors and power sources.

Next, we conclude and emphasize some basic properties of the potential function, which are easily ignored and were misunderstood in previous studies, such as [20], [21].

1) *The potential-based large-signal stability analysis is applicable to autonomous systems only.* It cannot be deployed in time-variant systems. The rule is constrained by LaSalle stability theorem [23], which builds mathematical foundation for the Brayton-Moser potential theory.

2) *The potential theory is preferred to be applied to complete circuits.* An incomplete circuit can be modified to a complete circuit by adding capacitors in parallel and inductors in series.

3) *The potential function is not a Lyapunov function or an energy function.* Being a Lyapunov function or energy function requires non-negativity. However, it can be concluded from the definition of the potential function that a potential function could be negative. The potential has the same unit as power. Suppose there is a nonlinear element whose voltage potential is $\eta = \int_0^{i_1} v_\mu di_\mu$. The dual function of voltage potential is $\zeta = \int_0^{v_1} i_\mu dv_\mu$, which is called current potential. The total power dissipation Ψ can be expressed as follows:

$$\Psi = i_1 v_1 = \int_0^{i_1} v_\mu di_\mu + \int_0^{v_1} i_\mu dv_\mu = \eta + \zeta \quad (19)$$

4) *The potential of a circuit depends only on the start point and end point of a motion trajectory, whereas it is independent of the trajectory itself.*

Generally, the Brayton-Moser potential theory provides the paramount method to analyze LSS in nonlinear circuit systems. However, it is not complete enough and is especially vulnerable when confronted with the stability problem in nonlinear systems with multiple equilibrium points. In this paper, we successfully resolve this dilemma by identifying hyperlocal stable equilibrium points and ROA estimation.

The potential function of the model in Fig. 6 is calculated as follows:

$$
\begin{aligned}
P(i, v) &= \sum_{i=1}^{N} V_{refi} \left(I_{pi} + I_{qi} \right) - \frac{1}{2} \sum_{i=1}^{N} R_{pi} I_{pi}^2 - \frac{1}{2} \sum_{i=1}^{N} R_{qi} I_{qi}^2 \\
&\quad - \frac{1}{2} \sum_{i=1}^{N} R_{ti} I_{ti}^2 - \frac{1}{2} \sum_{j=1}^{M} R_{fj} I_{fj}^2 - \sum_{i=1}^{N} V_{Ci} \left(I_{pi} + I_{qi} - I_{ti} \right) \\
&\quad - V_D \left(\sum_{i=1}^{N} I_{ti} - \sum_{j=1}^{M} I_{fj} \right) + \sum_{j=1}^{M} Z_j
\end{aligned}
\tag{20}
$$

where

$$
Z_j =
\begin{cases}
\int_{V_{min}}^{V_{Lj}} \frac{P_{Lj}}{v} dv - P_{Lj} - V_{Lj}(I_{fj} - I_{Lj}), & V_{Lj} > V_{\min\_j} \\
I_{\max\_j} \left(V_{Lj} - V_{\min\_j} \right) - P_{Lj} - V_{Lj}(I_{fj} - I_{\max\_j}), \\
\quad V_{Lj} \leq V_{\min\_j}
\end{cases}
\tag{21}
$$

I_{pi} and I_{qi} represent the currents through resistors R_{pi} and R_{qi}, respectively. V_{min} is the lower bound of the output voltage of CPL and I_{max} is the upper bound of current of CPL. Other notations are as marked in Fig. 6.

D. POTENTIAL-BASED STABILITY ANALYSIS OF MICROGRIDS

As for all the discussion of microgrid stability here, we first make the following two assumptions: (a) In the state equation of microgrid model described in (3), A^{-1} exists, (this always hold in our case and the explanation is presented in section IV.B); (b) there do exists equilibrium(s) in the microgrid model, that is, (10) is solvable. Conventional potential-based LSS analysis provides rigorous criteria for LSS in nonlinear systems. Every trajectory finally converges to a set notated by E when the stability criteria are satisfied, where E is the compact set consisting of *all equilibria* of the system. In fact, however, this conclusion indicates the unavoidable flaws of the traditional potential-based stability analysis in *multi-equilibria* systems. The traditional method only derives sufficient conditions for the convergence of trajectories to the set E but cannot reveal the equilibrium point to which it will exactly converge. An example is shown in Fig. 10(a). Suppose O is an initial point in a system defined in domain R^n; A, B, C are different equilibrium points of this system; and E is the compact set consisting of all equilibrium points, i.e., $E = \{A, B, C\}$. Then the sufficient conditions given by the traditional stability analysis are to ensure that the trajectory starting from O approaches E as $t \to \infty$. It is worth mentioning that this result involves three possible situations: the trajectory starting from O approaches equilibrium A, B, or C as $t \to \infty$.

In this paper, we propose a novel potential-based stability analysis to *differentiate* the convergences to different equilibrium points. This task is visualized as shown in Fig. 10(b). In the system domain $\mathcal{R}^n$, suppose O, O_1, O_2 are different

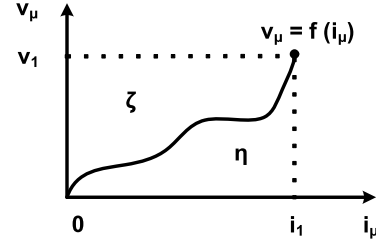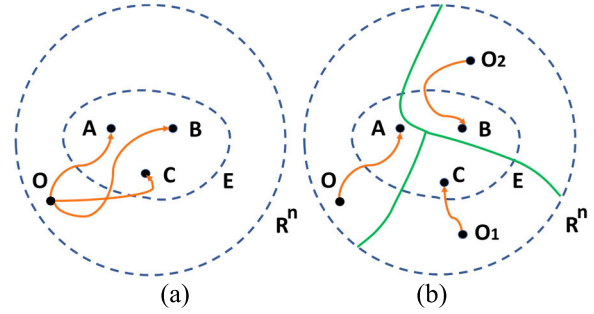FIGURE 9. **Potential functions of a nonlinear element.**

FIGURE 10. **Correspondence between initial conditions and equilibrium points.**

TABLE 2. **Comparison among different stability methods.**

Method/obtained information	Traditional potential-based method	Small-signal method	The proposed potential-based method
Global stability	✓	✗	✓
Local stability	✗	✓	✓

initial points; A, B, C are different equilibria of this system; and E is the compact set consisting of all equilibrium points, i.e., $E = \{A, B, C\}$. The HL-LSS of each equilibrium point is explored and the correspondence between initial conditions and converged equilibrium points is investigated. For example, it is concluded that the trajectory starting from O, O_1, O_2 converges to equilibrium A, B, C, respectively. Each equilibrium has a different ROA, which can be estimated using the proposed novel potential-based approach.

The following table shows the differences among the traditional potential-based method, the small-signal method, and our proposed novel method.

On the one hand, the novel proposed stability analysis overcomes the drawback of traditional potential-based analysis that cannot differentiate the convergence of trajectories with different initial conditions; on the other hand, the proposed novel stability analysis investigates both global stability and local stability, which is superior to other stability analysis methods.

The dynamic equation of the microgrid model in Fig. 6 is shown as follows:

$$
-J \frac{dx}{dt} = \frac{\partial P(x)}{\partial x}
\tag{22}
$$

where $x = [\, i\, v\,]^T$, $J = diag \left\{ \left[\, -L\ C\,\right] \right\}$.

$i = [I_{p1}, I_{p2}, \ldots, I_{pN}, I_{q1}, I_{q2}, \ldots, I_{qN}, I_{t1}, I_{t2}, \ldots, I_{tN},$
$I_{f1}, \ldots, I_{fM}]$,

$v = [V_{C1}, V_{C2}, \ldots, V_{CN}, V_L]$, L and C are the diagonal inductance matrix and the diagonal capacitance matrix, respectively. It is observed that whether J is positive definite is dependent on L and C under this description. We reconstruct the expression of this system to decouple this dependancy, which considers (P^*, J^*) instead of (P, J), such that

$$-J^* \frac{dx}{dt} = \nabla P^*(x) \qquad (23)$$

where J^* is positive definite in a stable system and ∇ is gradient operator. The pair (P^*, J^*) can be obtained by equation transformation and superposition:

$$J^* = \left(\lambda \mathbb{I} + \frac{\partial^2 P(x)}{\partial x^2} M \right) \cdot J, \; P^* = \lambda P + \frac{1}{2}\left(\frac{\partial P(x)}{\partial x}, M \frac{\partial P(x)}{\partial x} \right) \tag{24}$$

where $\mathbb{I}$ is an identity matrix, M is an arbitrary symmetric matrix, and λ is an arbitrary constant [16].

Theorem 1: Given a nonlinear circuit $\frac{dx}{dt} = f(x)$, as shown in Fig. 6, the potential-based dynamic function of the circuit is $-J^* \frac{dx}{dt} = \frac{\partial P^*(x)}{\partial x}$. Let $f : \mathcal{R}^n \to \mathcal{R}$ be a C^1 function and $P^* : \mathcal{R}^n \to \mathcal{R}$ be a C^2 function. D is a neighborhood of the equilibrium point x_e.

1-a: Suppose $J^* \succ 0$, $H(P^*)|_{x=x_e} \succ 0$, then x_e is a local minimum of P^* and an asymptotic stable equilibrium point [16]. [1]

1-b: For an asymptotic stable equilibrium x_e, there exists a Lyapunov function at $x = x_e$. The proof is presented in [17].

Theorem 1 presents sufficient conditions for HL-LSS of an equilibrium point and for the existence of a Lyapunov function. Furthermore, the existence of a Lyapunov function at an equilibrium point ensures the existence of the ROA at this equilibrium and is helpful in estimating the ROA.

V. POTENTIAL-BASED ROA ESTIMATION

ROA estimation is performed to differentiate the convergence of trajectories with different starting points. In this section, we propose a novel method to estimate the ROA of every equilibrium point where the conditions described in Theorem 1 are satisfied.

As introduced in section III.D, there exists a function $P^*(x)$ such that

$$\nabla P^*(x) = -J^* \dot{x} \qquad (25)$$

where $J^* \succ 0$, ∇ is the gradient operator, since $J^* \succ 0$, $(J^*)^{-1}$ exists. The above system can be equivalently formulated as:

$$\dot{x} = -(J^*)^{-1} \nabla P^*(x), \qquad (26)$$

The linearized system at equilibrium $x = x_e$ can be described in (27) and the original system can be described

---

[1] The notations "$\succ 0$" and "$\succeq 0$" represent positive definite and positive semi-definite, respectively. H is the Hessian matrix.

in (28).

$$\dot{\hat{x}} \approx -(J^*)^{-1} H(P^*)|_{x=x_e} \cdot \hat{x} = A\hat{x} \qquad (27)$$

$$\dot{\hat{x}} = A \cdot \hat{x} + g(\hat{x}) \qquad (28)$$

where H is the Hessian matrix, $A = -(J^*)^{-1} H(P^*)|_{x=x_e}$, $\hat{x} = x - x_e$, and $g(\hat{x}) = f(\hat{x} + x_e) - A\hat{x}$. The derivation is shown in Appendix A.

Theorem 2: Given a nonlinear circuit $\frac{dx}{dt} = f(x)$, as shown in Fig. 6, the potential-based dynamic function of the circuit is $-J^* \frac{dx}{dt} = \frac{\partial P^*(x)}{\partial x}$. Suppose $J^* \succ 0$, $H(P^*)|_{x=x_e} \succ 0$. From Theorem 1, we conclude that $x = x_e$ is an asymptotic stable equilibrium point and there exists a Lyapunov function at $x = x_e$. A Lyapunov function at $x = x_e$ can be constructed as follows:

$$L(x) = \hat{x}^T H(P^*)|_{x=x_e} \hat{x} \qquad (29)$$

where $\hat{x} = x - x_e$. The proof is presented in [17].

Theorem 2 provides a very convenient method to solve Lyapunov function for the microgrid dynamics. With potential-function-based modeling, we can use $H(P^*)|_{x=x_e}$ to construct the Lyapunov function directly. This characteristic reduces the computational costs in the traditional approach to solving Lyapunov equations. In traditional methods of solving Lyapunov function, it is not avoidable to solve matrix N given any symmetric and positive definite matrix Q. For example, the Hessenberg-Schur algorithm is utilized extensively to obtain a Lyapunov function, however, it greatly burdens the computation.

Consider the quadratic Lyapunov function $L(x)$ constructed in Theorem 2, i.e.

$$L = \hat{x}^T N \hat{x}, \qquad (30)$$

where $N = H(P^*)|_{x=x_e} \succ 0$, $\hat{x} = x - x_e$.

The derivative of Lyapunov function $L(x)$ is solved as follows:

$$\frac{dL}{dt} = -\hat{x}^T Q \hat{x} + 2\hat{x}^T N g(\hat{x}), \quad Q \succ 0 \qquad (31)$$

Since $\|g(\hat{x})\|_2 = o(\|\hat{x}\|_2)$, there exists $\gamma > 0$ such that

$$\forall \|\hat{x}\| \leq \gamma, \|g(\hat{x})\|_2 < \alpha \|\hat{x}\|_2 \qquad (32)$$

where $\alpha \in \mathcal{R}^+$.

The parameters γ and α can be determined as follows.

$$\alpha \leq \frac{\lambda_{min}(Q)}{2\lambda_{max}(N)} \qquad (33)$$

$$\gamma = \min_{j \in \{1,2,\ldots,M\}} \frac{V_{Lj}^*(Y_j - \sqrt{Y_j})}{Y_j - 1} \qquad (34)$$

where V_{Lj}^* is steady-state voltage of V_{Lj}, $Y_j = \alpha^2 \left(\frac{C_{fj}}{P_{Lj}} \right)^2 (V_{Lj}^*)^4$. It is worth mentioning that $Y_j < 1$ needs to be satisfied. This can be achieved by tuning α. The detailed derivation is developed in Appendix B.

It is not difficult to see that $D : \{\|\hat{x}\| \leq \gamma\}$ *cannot* be treated as an estimate of ROA directly. Even though a

TABLE 3. Simulation parameters (The unit: V, H, F, Ohm, W).

V_{ref1}	200	R_{p1}	5	R_{q1}	5	L_{q1}	0.1	C_{b1}	1
R_{t1}	8	L_{t1}	0.1	R_{f1}	5	L_{f1}	0.1	C_{f1}	1
V_{ref2}	200	R_{p2}	5	R_{q2}	5	L_{q2}	0.1	C_{b2}	1
R_{t2}	8	L_{t2}	0.1	R_{f2}	3	L_{f2}	0.1	C_{f2}	1
C_D	1	I_{max1}	∞	V_{min1}	0	I_{max2}	20	V_{min2}	20
P_{L1}	200	P_{L2}	400						

trajectory starting from D will go to the Lyapunov surface $L(x) = c_1$ from another Lyapunov surface $L(x) = c_2$, where $c_1, c_2 \in \mathcal{R}, c_1 < c_2$. It is not guaranteed that $L(x)$ will remain in D. Therefore, we should estimate the ROA by a compact set $\Omega_c \subset D$ such that every trajectory starting from Ω_c stays in Ω_c for all future moments. It can be determined that the set $\Omega_c = \{x \in \mathcal{R}^n, L(x) \le c\}$ is an ROA of the system, where c is defined as
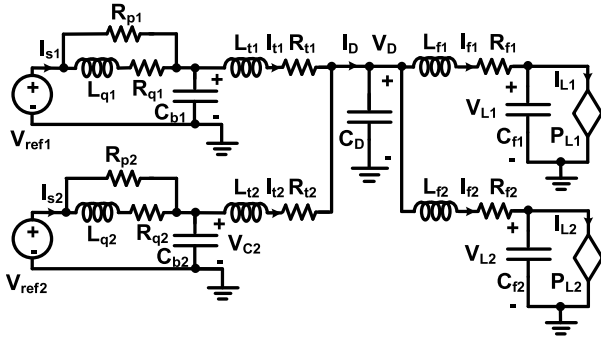
$$c \triangleq \min_{\|\hat{x}\|_2 = \gamma} x^T N x = \lambda_{min}(N)\gamma^2 \qquad (35)$$

N is set as $H(P^*)|_{x=x_e}$.

VI. CASE STUDY

To illustrate our proposed techniques, we investigate in this case study HL-LSS stability analysis and ROA estimation for DC microgrids with multiple equilibria.

Suppose there are two branches of power sources and two branches of loads. Then the equivalent circuit of the microgrid model can be shown as follows:

FIGURE 11. The equivalent circuit diagram of the microgrid model.

The simulation parameters are set as Table. 3. Load P_{L1} works as constant power mode; load P_{L2} works as constant power mode when voltage is higher than voltage bound V_{min2}, and works as constant current mode when voltage is lower than voltage bound V_{min2}.

A. STEADY-STATE ANALYSIS OF THE MICROGRID MODEL

Firstly we investigate Thevenin equivalence of the microgrid model for equilibrium analysis.

With the parameters in Table. 3., the parameters R_{eq} and V_{eq} of the Thevenin equivalent circuit are determined by

$$R_{eq} = \frac{1}{2} \cdot \left(\frac{R_{p1}R_{q1}}{R_{p1} + R_{q1}} + R_{t1} \right) \qquad (36)$$

$$V_{eq} = V_{s1} \qquad (37)$$

TABLE 4. Equilibrium points solved in the first case.

Equilibrium	1st	2nd	3rd	4th
I_{L1}^{*}	1.1338	15.4912	10.2877	3.1258
I_{L2}^{*}	2.2829	5.3914	14.3068	19.8052

Then we discuss the equilibrium points of the model by classification.

1) Suppose both load P_{L1} and load P_{L2} in the DC system work as constant power models. Then the power balancing equations of the system are as follows:

$$\begin{cases} P_{L1} = V_{eq} \cdot I_{L1} - I_{L1}^2 (R_{eq} + R_{f1}) - R_{eq}I_{L1}I_{L2} \\ P_{L2} = V_{eq} \cdot I_{L2} - I_{L2}^2 (R_{eq} + R_{f2}) - R_{eq}I_{L1}I_{L2} \end{cases} \qquad (38)$$

2) Suppose the load P_{L1} works as a constant power model and the load P_{L2} works as a constant current source. Then the Kirchhoff's circuit equations of the system are as follows:

$$\begin{cases} V_{L1} = V_{eq} - I_{L1} (R_{eq} + R_{f1}) - R_{eq}I_{max2} \\ I_{L2} = I_{max2} \end{cases} \qquad (39)$$

The above circuit equations (38)(39) are visualized in Fig. 13. It can be seen that there are six equilibrium points in total.
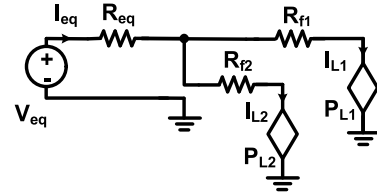
FIGURE 12. The Thevenin equivalent circuit model.
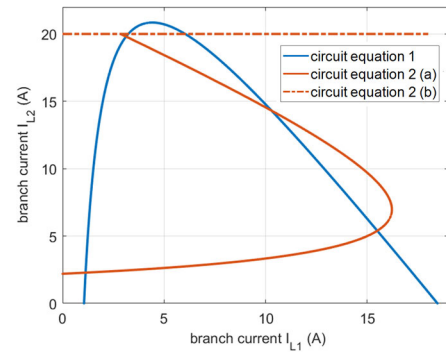
FIGURE 13. The equilibrium points in the microgrid model.

The equilibrium points in the first case are solved as follows.

The equilibrium points in the second case are solved as follows.

Second, we develop stability analysis for the equilibrium points to specify the stable one(s) among them using

TABLE 5. Equilibrium points solved in the second case.

Equilibrium	5th	6th
I_{L1}^*	6.0353	3.2330
V_{L2}^*	3.3149	18.0266

Theorem 1-a. The analysis results show that there are two stable equilibrium points: the first equilibrium point $(I_{L1}^*, I_{L2}^*) = (1.1338, 2.2829)$ and the 6th equilibrium point $(I_{L1}^*, V_{L2}^*) = (3.2330, 18.0266)$.

B. ROA ESTIMATION

We formulate the ROA estimation of the two stable equilibria in the microgrid model using our proposed approach.

1) Regarding the equilibrium $(I_{L1}^*, I_{L2}^*) = (1.1338, 2.2829)$, the steady-state load voltages are $(V_{L1}^*, V_{L2}^*) = (176, 175)$; the related parameters $\alpha = 0.0002, \gamma = 3.1690, c = 0.4490$. The estimated ROA is set $\Omega_{c1} = \{x \in \mathcal{R}^n, L(x) \leq 0.4490\}$. The estimated ROA is depicted in the subspace consisting of load voltage (V_{L1}, V_{L2}) in Fig. 14(a). The red dot marks the equilibrium point (i.e., the steady-state load voltages) and the blue ellipse plots the boundary of the estimated ROA.
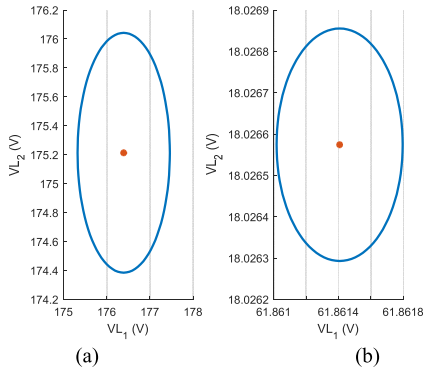

FIGURE 14. Auxiliary boundary in ROA estimation.

2) Regarding the second stable equilibrium point $(I_{L1}^*, V_{L2}^*) = (3.2330, 18.0266)$, the related parameters $\alpha = 0.00008, \gamma = 0.0014, c = 5.2711 \times 10^{-8}$. The estimated ROA is set as $\Omega_{c2} = \{x \in \mathcal{R}^n, L(x) \leq 5.2711 \times 10^{-8}\}$. The ROA is visualized in the subspace consisting of load voltage (V_{L1}, V_{L2}) in Fig. 14(b).

Next, we carry out simulations to verify the correctness of the ROA solved by the proposed theoretical method. We evaluate some typical scenarios which have the most extreme initial status of the microgrid model, such as the scenario with the largest current oscillation and the scenario with the largest voltage oscillation. We show the simulation-based verification at the data points with the maximum of $L(x)$. The results are shown in Fig. 15. Fig.15 (a) describes the case where both CPLs work under constant power mode; Fig. 15 (b) describes the case where one CPL works in constant power mode and the other CPL works in constant current mode. It can be
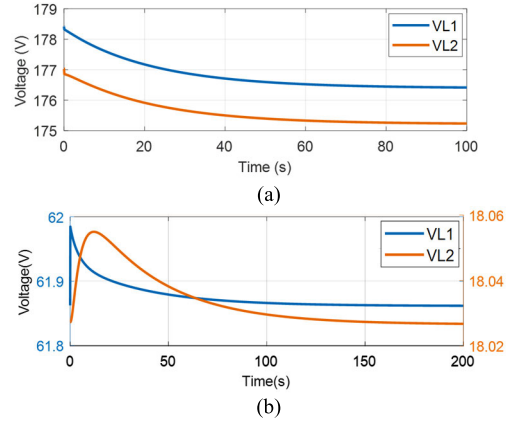

FIGURE 15. Dynamic responses of load voltages.

observed from Fig. 15 that the studied system converges to its equilibrium point in both cases as we expected in both cases.

VII. CONCLUSION AND FUTURE WORK

In this paper, we propose hyperlocal large-signal stability analysis from the perspective of potential theory in complex DC microgrids with multiple equilibrium points. On the one hand, we study the stability of each equilibrium and the convergence of state trajectories with different starting points; on the other hand, we estimate the multiple ROAs in microgrids with some strategies. Conventional potential theory is a flawed but creative and useful tool in large-signal stability analysis in nonlinear circuits. However, it has not been understood and facilitated precisely and completely in many past studies. Therefore, we correct the misunderstanding of potential theory and clarify related theoretical bases. Our future work will investigate more advanced ROA estimation methods with dimensionality reduction strategies. Deep reinforcement learning techniques might be utilized to reduce the curse of dimensionality [30], [31].

APPENDIX A

There exists a function $P^*(x)$ such that

$$\nabla P^*(x) = -J^* \dot{x} \tag{40}$$

where $J^* \succ 0, \nabla$ is the gradient operator, since $J^* \succ 0$, $(J^*)^{-1}$ exists. The above system can be equivalently formulated as:

$$\dot{x} = -(J^*)^{-1} \nabla P^*(x), \tag{41}$$

Linearize the system at equilibrium $x = x_e$:

$$\dot{\hat{x}} \approx - (J^*)^{-1} H(P^*)\big|_{x=x_e} \cdot \hat{x} = A\hat{x} \tag{42}$$

where H is the Hessian matrix, $A = - (J^*)^{-1} H(P^*)|_{x=x_e}$, and $\hat{x} = x - x_e$. Additionally, we have

$$\begin{aligned} \dot{\hat{x}} = \dot{x} &= - (J^*)^{-1} \nabla P^* (\hat{x} + x_e) \\ &= - (J^*)^{-1} H(P^*)\big|_{x=x_e} \cdot \hat{x} + g(\hat{x}) \\ &= A \cdot \hat{x} + g(\hat{x}) \end{aligned} \tag{43}$$

where $g(\hat{x}) = f(\hat{x} + x_e) - A\hat{x}$.

APPENDIX B

Consider the quadratic Lyapunov function $L(x)$ constructed in Theorem 2, i.e.

$$L = \hat{x}^T N \hat{x}, \tag{44}$$

where $N = H(P^*)|_{x=x_e} \succ 0, \hat{x} = x - x_e$. The derivative of Lyapunov function $L(x)$ is solved as follows:

$$\begin{aligned} \frac{dL}{dt} &= \dot{\hat{x}}^T N \hat{x} + \hat{x}^T N \dot{\hat{x}} \\ &= \left(\hat{x}^T A^T + g^T(\hat{x})\right) N \hat{x} + \hat{x}^T N \left(A\hat{x} + g(\hat{x})\right) \\ &= \hat{x}^T \left(A^T N + NA\right) \hat{x} + 2\hat{x}^T N g(\hat{x}) \\ &= -\hat{x}^T Q\hat{x} + 2\hat{x}^T N g(\hat{x}), Q \succ 0 \end{aligned} \tag{45}$$

Since $\|g(\hat{x})\|_2 = o(\|\hat{x}\|_2)$, there exists $\gamma > 0$ such that

$$\forall \|\hat{x}\| \le \gamma, \|g(\hat{x})\|_2 < \alpha \|\hat{x}\|_2 \tag{46}$$

where $\alpha \in \mathcal{R}^+$. Then

$$\begin{aligned} \frac{dL}{dt} &= -\hat{x}^T Q\hat{x} + 2(N^T\hat{x})^T g(\hat{x}) \\ &\le -\lambda_{min}(Q)\|\hat{x}\|^2 + 2\left\|N^T\hat{x}\right\|\|g(\hat{x})\| \\ &\le -\lambda_{min}(Q)\|\hat{x}\|^2 + 2\alpha\left\|N^T\hat{x}\right\|\|\hat{x}\| \\ &\le -\lambda_{min}(Q)\|\hat{x}\|^2 + 2\alpha\lambda_{max}(N)\|\hat{x}\|^2 \end{aligned} \tag{47}$$

To guarantee $\frac{dL}{dt} \le 0$, we set

$$-\lambda_{min}(Q)\|\hat{x}\|^2 + 2\alpha\lambda_{max}(N)\|\hat{x}\|^2 \le 0 \tag{48}$$

Therefore, α can be determined by the following equation:

$$\alpha \le \frac{\lambda_{min}(Q)}{2\lambda_{max}(N)} \tag{49}$$

Next, we can solve γ according to

$$\forall \|\hat{x}\| \le \gamma, \|g(\hat{x})\|_2 < \alpha \|\hat{x}\|_2 \tag{50}$$

We know

$$\begin{aligned} g(\hat{x}) &= f(\hat{x} + x_e) - A\hat{x} \\ &= \dot{x} + (J^*)^{-1} H(P^*)|_{x=x_e} \hat{x} \\ &= \dot{x} - \nabla f(x)|_{x=x_e} \hat{x} \end{aligned} \tag{51}$$

Denote the elements in vector $g(\hat{x})$ by $g_k(\widehat{x_k}), k = 1, 2, \ldots, N + M$. In fact, $g_k(\widehat{x_k}) = 0$ for variable $x_k : \dot{x}_k = f_k(x_k)$ if $f_k(x_k)$ is a linear function. In the type of microgrids proposed in this paper, the variables $I_{pi}, I_{qi}, I_{ti}, I_{fj}, V_{Ci}(i = 1, 2, \ldots, N, j = 1, 2, \ldots, M)$ are subject to this situation. However, $g_k(\widehat{x_k}) \ne 0$ for variables $V_{Lj}(j = 1, 2, \ldots, M)$ considering these variables correspond to nonlinear functions. Consider we have

$$\dot{V}_{Lj} = f_k(x) = \frac{1}{C_{fj}}(i_{fj} - \frac{P_{Lj}}{V_{Lj}}) \tag{52}$$

We can calculate $g_k\left(\widehat{V}_{Lj}\right)$ as follows:

$$\begin{aligned} g_k\left(\widehat{V}_{Lj}\right) &= \dot{V}_{Lj} - \nabla f_k(x)|_{V_{Lj}=V_{Lj}^*} \cdot \hat{x} \\ &= -\frac{P_{Lj}\widehat{V}_{Lj}^2}{(V_{Lj}^* + \widehat{V}_{Lj})C_{fj}(V_{Lj}^*)^2} \end{aligned} \tag{53}$$

where V_{Lj}^* is steady-state voltage of V_{Lj}. Then we solve

$$\|g(\hat{x})\|_2 < \alpha \|\hat{x}\|_2 \tag{54}$$

The above inequality can be guaranteed if

$$\left\|g_k\left(\widehat{V}_{Lj}\right)\right\|_2 < \alpha \left\|\widehat{V}_{Lj}\right\|_2, \quad \forall j = 1, 2, \ldots, M \tag{55}$$

Solving this inequality, we obtain

$$\widehat{V}_{Lj} = \frac{V_{Lj}^*(-Y_j \pm \sqrt{Y_j})}{Y_j - 1}, \quad \forall j = 1 \ldots M \tag{56}$$

where

$$Y_j = \alpha^2 (\frac{C_{fj}}{P_{Lj}})^2 (V_{Lj}^*)^4 \tag{57}$$

It is worth mentioning that $Y_j < 1$ needs to be satisfied. This can be achieved by tuning α. Then γ can be determined based on its definition as follows:

$$\gamma = \min_{j \in \{1,2,\ldots,M\}} \frac{V_{Lj}^*(Y_j - \sqrt{Y_j})}{Y_j - 1} \tag{58}$$

REFERENCES

[1] M. Stieneker and R. W. De Doncker, "Medium-voltage DC distribution grids in urban areas," in *Proc. IEEE 7th Int. Symp. Power Electron. Distrib. Gener. Syst. (PEDG)*, Vancouver, BC, Canada, Jun. 2016, pp. 1–7.

[2] H. Bevrani, T. Ise, and Y. Miura, "Virtual synchronous generators: A survey and new perspectives," *Int. J. Electr. Power Energy Syst.*, vol. 54, pp. 244–254, Jan. 2014.

[3] Z. Shuai *et al.*, "Microgrid stability: Classification and a review," *Renew. Sustain. Energy Rev.*, vol. 58, pp. 167–179, May 2016.

[4] Y. Yang, C. Li, J. Xu, F. Blaabjerg, and T. Dragicevic, "Virtual inertia control strategy for improving damping performance of DC microgrid with negative feedback effect," *IEEE J. Emerg. Sel. Topics Power Electron.*, vol. 9, no. 2, pp. 1241–1257, Apr. 2021.

[5] N. Rashidirad, M. Hamzeh, K. Sheshyekani, and E. Afjei, "A simplified equivalent model for the analysis of low-frequency stability of multi-bus DC microgrids," *IEEE Trans. Smart Grid*, vol. 9, no. 6, pp. 6170–6182, Nov. 2018.

[6] M. Lu, X. Wang, P. C. Loh, and F. Blaabjerg, "Resonance interaction of multiparallel grid-connected inverters with LCL filter," *IEEE Trans. Power Electron.*, vol. 32, no. 2, pp. 894–899, Feb. 2017.

[7] M. Belkhayat, "Stability criteria for AC power systems with regulated loads with regulated loads," Ph.D. dissertation, Dept. Elect. Eng., Purdue Univ., West Lafayette, IN, USA, 1997.

[8] M. Céspedes, T. Beechner, L. Xing, and J. Sun, "Stabilization of constant-power loads by passive impedance damping," in *Proc. 25th Annu. IEEE Appl. Power Electron. Conf. Expo. (APEC)*, Feb. 2010, pp. 2174–2180.

[9] M. Su, Z. Liu, Y. Sun, H. Han, and X. Hou, "Stability analysis and stabilization methods of DC microgrid with multiple parallel-connected DC–DC converters loaded by CPLs," *IEEE Trans. Smart Grid*, vol. 9, no. 1, pp. 132–142, Jan. 2018.

[10] X. Lu, K. Sun, J. M. Guerrero, J. C. Vasquez, L. Huang, and J. Wang, "Stability enhancement based on virtual impedance for DC microgrids with constant power loads," *IEEE Trans. Smart Grid*, vol. 6, no. 6, pp. 2770–2783, Nov. 2015.

[11] S. Anand and B. G. Fernandes, "Reduced-order model and stability analysis of low-voltage DC microgrid," *IEEE Trans. Ind. Electron.*, vol. 60, no. 11, pp. 5040–5049, Nov. 2013.

[12] D. Marx, P. Magne, B. Nahid-Mobarakeh, S. Pierfederici, and B. Davat, "Large signal stability analysis tools in DC power systems with constant power loads and variable power loads—A review," *IEEE Trans. Power Electron.*, vol. 27, no. 4, pp. 1773–1787, Apr. 2012.

[13] P. Magne, B. Nahid-Mobarakeh, and S. Pierfederici, "DC-link voltage large signal stabilization and transient control using a virtual capacitor," in *Proc. IEEE Ind. Appl. Soc. Annu. Meeting*, Houston, TX, USA, Oct. 2010, pp. 1–8.

[14] T. Takagi and M. Sugeno, "Fuzzy identification of systems and its applications to modeling and control," in *Readings in Fuzzy Sets for Intelligent Systems*. San Mateo, CA, USA: Kaufmann, 1993, pp. 387–403.

[15] K. A. Potty, E. Bauer, H. Li, B. Hu, and J. Wang, "Smart resistor: Dynamic stabilization of constant power loads in DC microgrids with high bandwidth power converters and energy storage," in *Proc. IEEE Appl. Power Electron. Conf. Expo. (APEC)*, Tampa, FL, USA, Mar. 2017, pp. 2795–2801.

[16] R. K. Brayton and J. K. Moser, "A theory of nonlinear networks. I," *Quart. Appl. Math.*, vol. 22, no. 1, pp. 1–33, 1964.

[17] F. Chang, X. Cui, M. Wang, and W. Su, "Region of attraction estimation for DC microgrids with constant power loads using potential theory," *IEEE Trans. Smart Grid*, vol. 12, no. 5, pp. 3793–3808, Sep. 2021.

[18] M. Belkhayat, R. Cooley, and A. Witulski, "Large signal stability criteria for distributed systems with constant power loads," in *Proc. Power Electron. Spec. Conf. (PESC)*, Jun. 1995, pp. 1333–1338.

[19] A. Griffo and J. Wang, "Large signal stability analysis of 'more electric' aircraft power systems with constant power loads," *IEEE Trans. Aerosp. Electron. Syst.*, vol. 48, no. 1, pp. 477–489, Jan. 2012.

[20] W. Du, J. Zhang, Y. Zhang, and Z. Qian, "Stability criterion for cascaded system with constant power load," *IEEE Trans. Power Electron.*, vol. 28, no. 4, pp. 1843–1851, Apr. 2013.

[21] D. Peng, M. Huang, J. Li, J. Sun, X. Zha, and C. Wang, "Large-signal stability criterion for parallel-connected DC–DC converters with current source equivalence," *IEEE Trans. Circuits Syst. II, Exp. Briefs*, vol. 66, no. 12, pp. 2037–2041, Dec. 2019.

[22] F. Chang, X. Cui, M. Wang, W. Su, and A. Q. Huang, "Large-signal stability criteria in DC power grids with distributed-controlled converters and constant power loads," *IEEE Trans. Smart Grid*, vol. 11, no. 6, pp. 5273–5287, Nov. 2020.

[23] H. K. Khalil, *Nonlinear Systems*. Upper Saddle River, NJ, USA: Prentice-Hall, 2002, p. 128.

[24] X. Cui and A.-T. Avestruz, "Switching-synchronized sampled-state space modeling and digital controller for a constant off-time, current-mode boost converter," in *Proc. Amer. Control Conf. (ACC)*, Philadelphia, PA, USA, Jul. 2019, pp. 626–633.

[25] *Superposition Theorem*. Accessed: Jun. 2017. [Online]. Available: https://en.wikipedia.org/wiki/Superposition_theorem

[26] N. Barabanov, R. Ortega, R. Griñó, and B. Polyak, "On existence and stability of equilibria of linear time-invariant systems with constant power loads," *IEEE Trans. Circuits Syst. I, Reg. Papers*, vol. 63, no. 1, pp. 114–121, Jan. 2016.

[27] Z. Liu, M. Su, Y. Sun, W. Yuan, H. Han, and J. Feng, "Existence and stability of equilibrium of DC microgrid with constant power loads," *IEEE Trans. Power Syst.*, vol. 33, no. 6, pp. 6999–7010, Nov. 2018.

[28] W. Millar, "CXVI. Some general theorems for non-linear systems possessing resistance," *London, Edinburgh, Dublin Phil. Mag. J. Sci.*, vol. 42, no. 333, pp. 1150–1160, Oct. 1951.

[29] H. K. Khalil, *Nonlinear Systems*. Upper Saddle River, NJ, USA: Prentice-Hall, 2002, pp. 136–139.

[30] M. Landajuela *et al.*, "Discovering symbolic policies with deep reinforcement learning," in *Proc. 38th Int. Conf. Mach. Learn.*, Jul. 2021, pp. 5979–5989.

[31] R. Glatt and A. Costa, "Improving deep reinforcement learning with knowledge transfer," in *Proc. AAAI Conf. Artif. Intell.*, Feb. 2017, vol. 31, no. 1, pp. 1–2.

FANGYUAN CHANG (Graduate Student Member, IEEE) received the B.S. degree in electrical engineering from North China Electric Power University, China, in 2016, and the M.S. degree in electrical engineering from the University of Michigan, Ann Arbor, MI, USA, in 2018. She is currently pursuing the Ph.D. degree with the University of Michigan-Dearborn, Dearborn, MI, USA. Her research interests include power systems, control theory, and machine learning.
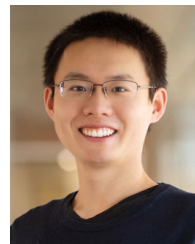
XIAOFAN CUI (Graduate Student Member, IEEE) received the B.S. degree in electrical engineering and automation from Tsinghua University in 2016. He is currently pursuing the Ph.D. degree in electrical engineering and computer science with the University of Michigan, Ann Arbor. He was a Visiting Student at Standard University during the Summer of 2015. His research interests include circuit modeling, digital control, and high-performance power electronics.
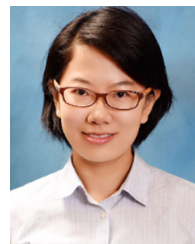
MENGQI WANG (Senior Member, IEEE) received the B.S. degree in electrical engineering from Xi'an Jiaotong University, Xi'an, in 2009, and the Ph.D. degree in electrical engineering from North Carolina State University, Raleigh, NC, USA, in 2014. Since 2015, she has been an Assistant Professor with the Department of Electrical and Computer Engineering, University of Michigan-Dearborn, USA. Her current research interests include DC-DC and DC-AC power conversions, high efficiency and high power-density power supplies, renewable energy systems, and wide-bandgap power device applications.

WENCONG SU (Senior Member, IEEE) received the B.S. degree (Hons.) from Clarkson University, Potsdam, NY, USA, in 2008, the M.S. degree from Virginia Tech, Blacksburg, VA, USA, in 2009, and the Ph.D. degree from North Carolina State University, Raleigh, NC, USA, in 2013. He is currently an Associate Professor with the Department of Electrical and Computer Engineering, University of Michigan-Dearborn, USA. His current research interests include power systems, electrified transportation systems, and cyber-physical systems. He is a registered Professional Engineer (P.E.) with the State of Michigan, USA. He is a fellow of IET. He is an Editor of IEEE Transactions on Smart Grid and an Associate Editor of IEEE Access.

• • •